

Diffusively Anisotropic Model for the Deflagration-to-Detonation Transition

Leonid Kagan and Gregory Sivashinsky
School of Mathematical Sciences, Tel Aviv University,
Tel Aviv 69978, Israel

Abstract

For elucidation of the key mechanisms responsible for the transition from deflagrative to detonative combustion in smooth-walled channels, a reactive flow with anisotropic thermal and molecular diffusivities is considered. Setting the transverse diffusivities large compared to longitudinal diffusivities the initially formed deflagration (despite no-slip boundary conditions) appears to be nearly planar and not accelerating. This however does not prevent its eventual abrupt transition to the Chapman-Jouguet detonation.

1 Introduction

Understanding of the key interactions controlling deflagration-to-detonation transition (DDT) remains one of the major challenges of combustion theory. Premixed gas combustion in smooth-walled channels is apparently the simplest system for studying the DDT. Yet, even in this geometry the emerging dynamical picture is too complex for straightforward identification of the mechanisms involved.

In the traditional attempt to explain the transition, the role of confinement is reduced exclusively to a generation of hydrodynamic disturbances (turbulence). The latter promotes extension of the flame interface resulting in the flame acceleration and enhancement of the flame-supported compression waves, which allegedly leads to formation of hot-spots triggering localized explosions and transition to detonation [1]. Yet, recently it was realized that there is a complementary aspect of the flame-confinement interaction. Apart from inducing hydrodynamic disturbances, the confinement also exerts resistance to the gas flow, causing local precompression of the premixture resulting in its preheating and autoignition. The resistance appears to be an agency perfectly capable of provoking the DDT even if the predetonation acceleration due to flame folding is deliberately suppressed and the system is regarded as effectively one-dimensional [2]. In this approach, the confinement is accounted for phenomenologically through the velocity-dependent drag-force term added to the momentum equation, while leaving the equation for energy balance unaltered (Fanno's hydraulic resistance model [3]).

As the Fanno model is not a rational approximation, its success should be perceived only as a good argument in support of the resistance concept, rather than a definite proof.¹ In real-world systems,

¹An attempt to put the Fanno model on a solid theoretical foundation for narrow channels has recently been undertaken in [4].

the interface extension and hydraulic resistance are invariably entangled, which makes the cause-effect analysis very difficult. A rational isolation of elementary mechanisms is often attained as some of the system's parameters approach their limits. In the absence of a suitable small parameter, to split apart a complex process, it is sometimes helpful to introduce an entirely artificial (book-keeping) parameter of expansion. This is precisely the strategy we intend to adopt.

2 Formulation

Let us artificially make the system diffusively anisotropic. Specifically, we'll keep the kinematic viscosity isotropic while setting the transverse thermal and molecular diffusivities large compared to their longitudinal counterparts and viscosity.

In suitably chosen units the set of modified Navier-Stokes equations for a compressible reactive flow then reads (cf. [5]),

continuity and state,

$$\frac{\partial \hat{\rho}}{\partial \hat{t}} + \frac{\partial \hat{\rho} \hat{u}}{\partial \hat{x}} + \frac{\partial \hat{\rho} \hat{v}}{\partial \hat{y}} = 0, \quad \hat{P} = \hat{\rho} \hat{T}, \quad (1)$$

momentum,

$$\hat{\rho} \left(\frac{\partial \hat{u}}{\partial \hat{t}} + \hat{u} \frac{\partial \hat{u}}{\partial \hat{x}} + \hat{v} \frac{\partial \hat{u}}{\partial \hat{y}} \right) + \frac{1}{\gamma} \frac{\partial \hat{P}}{\partial \hat{x}} = \epsilon Pr \left[2 \frac{\partial^2 \hat{u}}{\partial \hat{x}^2} + \frac{\partial}{\partial \hat{y}} \left(\frac{\partial \hat{u}}{\partial \hat{y}} + \frac{\partial \hat{v}}{\partial \hat{x}} \right) - \frac{2}{3} \frac{\partial}{\partial \hat{x}} \left(\frac{\partial \hat{u}}{\partial \hat{x}} + \frac{\partial \hat{v}}{\partial \hat{y}} \right) \right], \quad (2)$$

$$\hat{\rho} \left(\frac{\partial \hat{v}}{\partial \hat{t}} + \hat{u} \frac{\partial \hat{v}}{\partial \hat{x}} + \hat{v} \frac{\partial \hat{v}}{\partial \hat{y}} \right) + \frac{1}{\gamma} \frac{\partial \hat{P}}{\partial \hat{y}} = \epsilon Pr \left[2 \frac{\partial^2 \hat{v}}{\partial \hat{y}^2} + \frac{\partial}{\partial \hat{x}} \left(\frac{\partial \hat{u}}{\partial \hat{y}} + \frac{\partial \hat{v}}{\partial \hat{x}} \right) - \frac{2}{3} \frac{\partial}{\partial \hat{y}} \left(\frac{\partial \hat{u}}{\partial \hat{x}} + \frac{\partial \hat{v}}{\partial \hat{y}} \right) \right], \quad (3)$$

heat,

$$\begin{aligned} \frac{1}{\gamma} \hat{\rho} \left(\frac{\partial \hat{T}}{\partial \hat{t}} + \hat{u} \frac{\partial \hat{T}}{\partial \hat{x}} + \hat{v} \frac{\partial \hat{T}}{\partial \hat{y}} \right) + \left(\frac{\gamma - 1}{\gamma} \right) \hat{P} \left(\frac{\partial \hat{u}}{\partial \hat{x}} + \frac{\partial \hat{v}}{\partial \hat{y}} \right) = \\ \epsilon \left(\frac{\partial^2 \hat{T}}{\partial \hat{x}^2} + \alpha \frac{\partial^2 \hat{T}}{\partial \hat{y}^2} \right) + (\gamma - 1) \epsilon Pr \hat{\Phi} + (1 - \sigma_p) \hat{W}, \end{aligned} \quad (4)$$

where

$$\hat{\Phi} = 2 \left(\frac{\partial \hat{u}}{\partial \hat{x}} \right)^2 + 2 \left(\frac{\partial \hat{v}}{\partial \hat{y}} \right)^2 + \left(\frac{\partial \hat{v}}{\partial \hat{x}} + \frac{\partial \hat{u}}{\partial \hat{y}} \right)^2 - \frac{2}{3} \left(\frac{\partial \hat{u}}{\partial \hat{x}} + \frac{\partial \hat{v}}{\partial \hat{y}} \right)^2, \quad (5)$$

concentration,

$$\hat{\rho} \left(\frac{\partial \hat{C}}{\partial \hat{t}} + \hat{u} \frac{\partial \hat{C}}{\partial \hat{x}} + \hat{v} \frac{\partial \hat{C}}{\partial \hat{y}} \right) = \frac{\epsilon}{Le} \left(\frac{\partial^2 \hat{C}}{\partial \hat{x}^2} + \alpha \frac{\partial^2 \hat{C}}{\partial \hat{y}^2} \right) - \hat{W}, \quad (6)$$

chemical kinetics,

$$\hat{W} = Z \hat{\rho}^2 \hat{C} \exp \left(N_p (1 - \hat{T}^{-1}) \right) \quad (7)$$

Here α is the anisotropy factor; $\hat{P} = P/P_0$ is the scaled pressure in units of the initial pressure, P_0 ; $\hat{C} = C/C_0$, scaled concentration of the deficient reactant in units of its initial value, C_0 ; $\hat{T} = T/T_p$, scaled temperature in units of $T_p = T_0 + Q C_0 / c_p$, adiabatic the temperature of burned gas under constant pressure, P_0 ; T_0 is the initial temperature of unburned gas; Q , heat release; $\sigma_p = T_0/T_p$; $\gamma = c_p/c_v$; c_p , c_v , specific heats; $\epsilon = (u_p/a_p)^2$, scaled longitudinal thermal diffusivity, where u_p , velocity of the free-space (isobaric) deflagration relative to the burned gas is regarded as a prescribed parameter;

$a_p = \sqrt{\gamma(c_p - c_v)T_p}$, $a_0 = \sqrt{\gamma(c_p - c_v)T_0}$, sonic velocities at $T = T_p$ and $T = T_0$, respectively; $(\hat{u}, \hat{v}) = (u, v)/a_p$, scaled flow velocity; $N_p = E/RT_p$, scaled activation energy; $\hat{\rho} = \rho/\rho_p$, where $\rho_p = P_0/(c_p - c_v)T_p$, density of the combustion products in free-space deflagration; $\hat{t} = t/t_p$, $(\hat{x}, \hat{y}) = (x, y)/x_p$, $x_p = a_p t_p$, where $t_p = A^{-1}Z \exp(N_p)$ is the reference time; $Z = \frac{1}{2}Le^{-1}N_p^2(1 - \sigma_p)^2$ is the normalizing factor to ensure that at $N_p \gg 1$ and adiabatic free-space conditions the scaled deflagration velocity relative to the burned gas is close to $\sqrt{\epsilon}$; A , pre-exponential factor; Pr , Le - are the Prandtl and Lewis numbers, respectively. In the adopted formulation the molecular transport coefficients as well as specific heats are assumed to be constant.

As may be readily shown, $x_p = a_p t_p = l_{th}/\sqrt{\epsilon}$, where $l_{th} = D_{th}^p/u_p$ is the flame width; D_{th}^p , thermal diffusivity at $T = T_p$.

The reaction rate (7) is modeled by a single step Arrhenius kinetics. The latter is assumed to be of the first order with respect to the deficient reactant and of the second order with respect to the density, to account for the binary nature of chemical reaction taking place in real combustion systems.

Eqs (1)-(7) are considered over a strip $0 < \hat{x} < \infty$, $-\hat{d}/2 < \hat{y} < \hat{d}/2$, and subjected to the adiabatic and non-slip boundary conditions, and closed-end ignition (initial) conditions [5,6].

3 Numerical simulations

To avoid too large a disparity between the spatio-temporal scales involved, the numerical simulations are conducted for a thin channel and reduced values of the activation energy N_p and the inverse Mach number a_p/u_p , compared to those typical of real-life explosives. Specifically, we set,

$$N_p = 4, \quad a_p/u_p = 10, \quad \sigma_p = 0.2, \quad Le = 1, \quad Pr = 0.75, \quad \gamma = 1.3, \quad (8)$$

$$\hat{l} = 0.1, \quad \hat{d} = 1 \quad \alpha = 1, 10, 15, 20, 30, 100.$$

For the chosen parameter set the channel's width is $1/\sqrt{\epsilon} = 10$ -times the flame width l_{th} . The flame burning velocity $u_0 = \sigma_p u_p$ is $\sqrt{\epsilon\sigma_p} = 0.045$ -times the unburned gas sonic velocity a_0 .

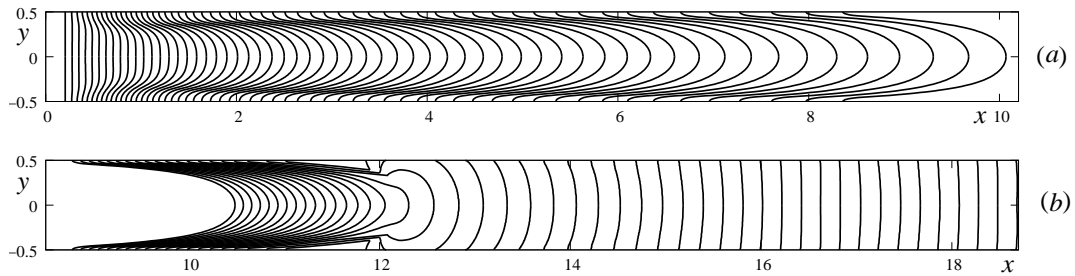


Figure 1: Isotropic case ($\alpha = 1$). Reaction zone configurations (maximum \hat{W}) at several consecutive equidistant instants of time. Frame (a) corresponds to deflagrative burning; $0 < \hat{t} < 30$, $\Delta\hat{t} = 0.5$. Frame (b) covers the transition event; $30 < \hat{t} < 34.6$, $\Delta\hat{t} = 0.1$. Note the islands of unburned gas formed near the wall immediately after the autoignition event (see also [6]). In all the figures, the hats on the labels have been omitted.

The computational method used and its validation are described in [5].

Some results of numerical simulations are depicted on Figs. 1-6.

Figures 1,2 show configurations of the reaction zone at several consecutive instants of time for the isotropic and strongly anisotropic cases. Figures 3,4 show the longitudinal profiles of pressure, temperature, density, and flow-velocity at several equidistant instants of time adjacent to the transition point.

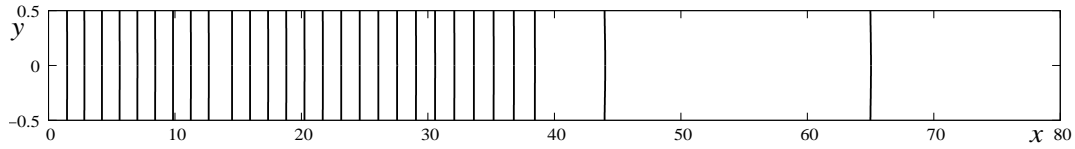


Figure 2: Anisotropic case ($\alpha = 100$). Reaction zone configurations at several consecutive equidistant instants of time: $0 < \hat{t} < 290$, $\Delta\hat{t} = 10$. Note the disparity between the transverse and longitudinal scales (10-fold compression)

Figure 5 shows flow-fields at two instants of time adjacent to the transition point. Figure 6 shows time-records for the reaction-wave propagation velocities at different levels of the anisotropy.

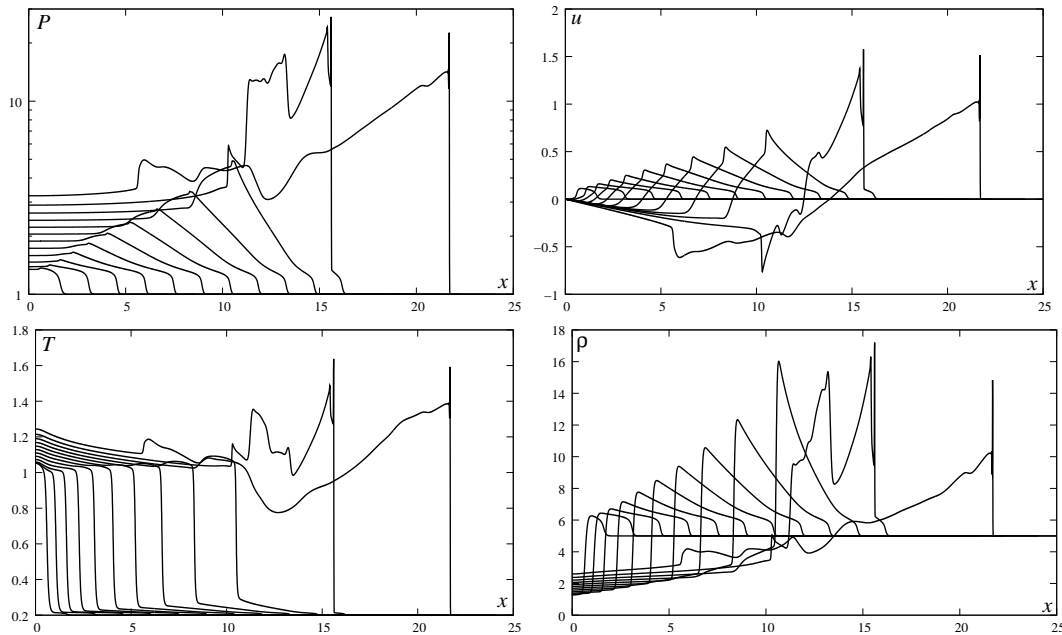


Figure 3: Isotropic case ($\alpha = 1$). Profiles of the scaled pressure \hat{P} , temperature \hat{T} , flow-velocity \hat{u} , and density $\hat{\rho}$ along the channel's symmetry plane ($\hat{y} = 0$) at several equidistant instants of time; $0 < \hat{t} < 36$, $\Delta\hat{t} = 3$.

4 Discussion

At high anisotropy ($\alpha = 100$), due to no-slip boundary conditions, the developing flow preserves its two-dimensional nature (Fig. 5). However, owing to strong transverse diffusivities the emerging temperature and concentration fields become nearly one-dimensional². As a result the initially formed deflagration appears to be nearly planar and not accelerating. This however does not prevent the eventual DDT, although the corresponding DDT-time and distance are considerably longer than in the isotropic case where the flame is folded and accelerates virtually from the moment of its inception (Fig.6).

Upon the transition (irrespective of the anisotropy) the detonation velocity settles at the same level given by the classical Chapman-Jouguet relation,

$$D \simeq \sqrt{2(\gamma^2 - 1)QC_0} \quad (9)$$

²The corresponding iso-lines are just straight lines orthogonal to the channel's walls, and being not very informative, are not shown here.

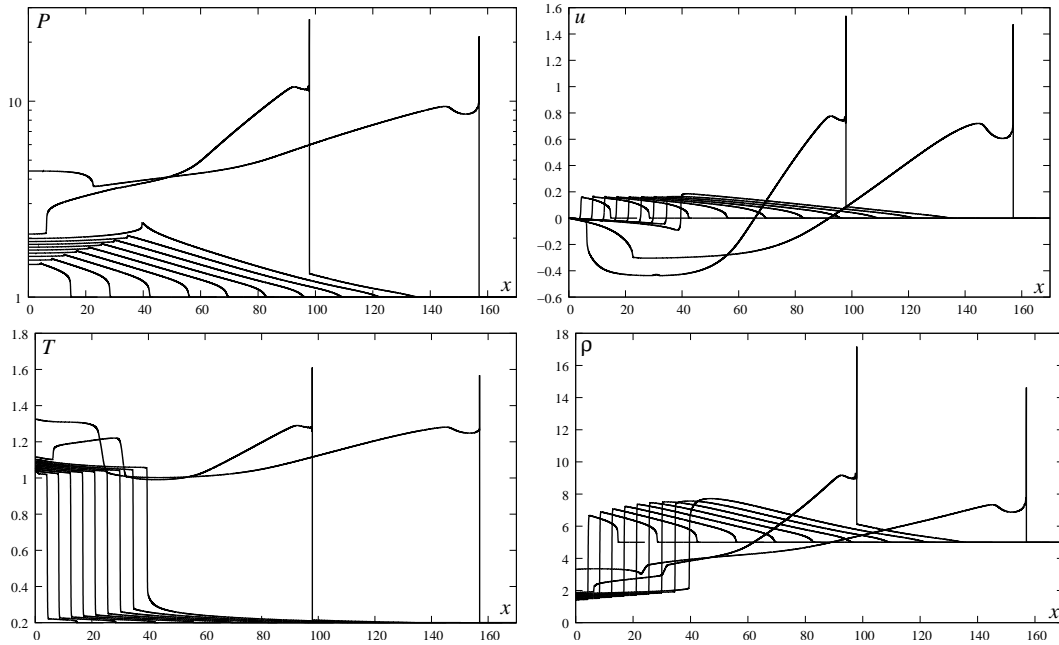


Figure 4: Anisotropic case ($\alpha = 100$). See the caption for Fig. 3; $0 < \hat{t} < 330$, $\Delta \hat{t} = 30$.

or in the scaled form,

$$\hat{D} \simeq \sqrt{2(\gamma + 1)(1 - \sigma_p)} = 1.918 \quad (10)$$

The above observations clearly lend extra weight to the assertion that the flame-folding and acceleration are not crucial for the transition, although they certainly help.

It is interesting that similar suppression of the flame-folding and acceleration may be achieved for the familiar limit of small-heat-release [7].

Accounting for heat losses by adopting, for example, Newton boundary conditions will complicate the picture: an effective suppression of the folding will be blocked. Moreover, at a large α a self-sustained combustion spread will become unfeasible. Yet at a moderate α , in line with the isotropic case [6,8], the DDT-time will increase.

Acknowledgments

These studies were supported by the Bauer-Neumann Chair in Applied Mathematics and Theoretical Mechanics, the US-Israel Binational Science Foundation (Grant 2006-151), and the Israel Science Foundation (Grant 32/09).

References

- [1] Oran E.S., Gamezo V.N. (2007). *Combust. Flame* 148: 4-47.
- [2] Brailovsky I., Sivashinsky S. (2000). *Combust. Flame* 122: 130-138.
- [3] Ward-Smith A.J. *Internal fluid flow: the fluid dynamics of flow in pipes and ducts*, Oxford Univ. Press, New York, 1980
- [4] Kagan L., Sivashinsky G. in *Proc.European Combust.Meeting, Lund,Sweden,25-28 June 2013*.

[5] Kagan L., Sivashinsky G. (2003). Combust. Flame 134: 389-397.

[6] Kagan L. (2007). Math. Model. Nat. Phenom. 2: 40-55.

[7] Brailovsky I., Kagan L., Sivashinsky G. (2012). Phil. Trans. R. Soc., A 370: 625-646.

[8] Kagan L., Sivashinsky, G. (2010). Flow Turbulence Combust. 84: 423-437

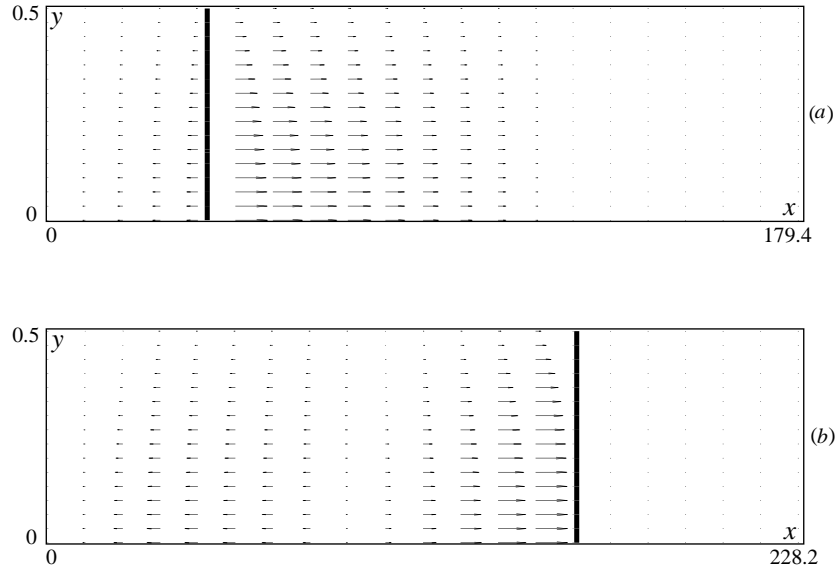


Figure 5: Advancing reaction zone (bold line) and the induced flow field at two instants of time adjacent to the transition event; (a) $\hat{t} = 261$ - deflagration, (b) $\hat{t} = 331$ - detonation.

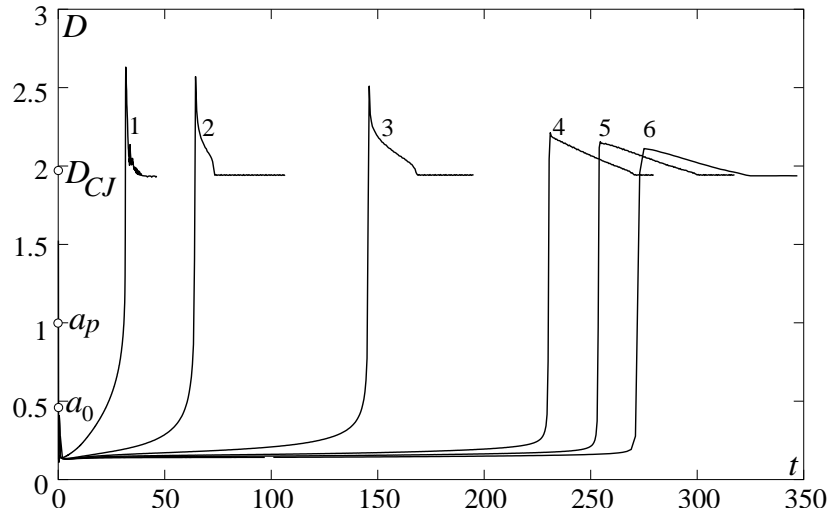


Figure 6: Temporal evolution of the reaction wave propagation velocity at different levels of anisotropy: $\alpha = 1$ (1), $\alpha = 10$ (2), $\alpha = 15$ (3), $\alpha = 20$ (4), $\alpha = 30$ (5), $\alpha = 100$ (6); \hat{D}_{CJ} corresponds to the Chapman-Jouguet detonation, \hat{a}_0, \hat{a}_p - to the sonic velocities in fresh and burned gas, respectively.